Parasitic phases at the origin of magnetic moment in $BiFeO_3$ thin films grown by low deposition rate RF sputtering

Thiago J. A. Mori,[1,a)] Caroline L. Mouls,[1,2] Felipe F. Morgado,[1,3] Pedro Schio,[1] and Júlio C. Cezar[1]

[1]*Laboratório Nacional de Luz Síncrotron, Centro Nacional de Pesquisa em Energia e Materiais, Campinas, SP 13083-970, Brazil*
[2]*Instituto de Física Gleb Wataghin, Universidade Estadual de Campinas, Campinas, SP 13083-859, Brazil*
[3]*Instituto de Física de São Carlos, Universidade Estadual de São Paulo, São Carlos, SP 13566-590, Brazil*

(Received 16 March 2017; accepted 6 September 2017; published online 22 September 2017)

A series of epitaxial $BiFeO_3$ thin films has been grown under high partial pressure in a pure O_2 atmosphere, which leads to a low deposition rate. The samples grown under these conditions have presented an evolution of the quality of the epitaxy as the deposition temperature increases, however, spurious β–Bi_2O_3 and supertetragonal $BiFeO_3$ phases are present in the films grown at higher temperatures. The presence of γ–Fe_2O_3 is reported in one growing condition, and has been attributed to the origin of hysteretic ferromagnetic behavior. A second kind of magnetism, with higher magnetic moment and anhysteretic behaviour, is attributed to the presence of mixed phases of $BiFeO_3$. *Published by AIP Publishing*. [http://dx.doi.org/10.1063/1.5003764]

I. INTRODUCTION

Materials which present simultaneously two or more ferroic orders are called multiferroics.[1] Among these, magnetoelectric materials possess both magnetic (ferro- and/or antiferromagnetism) and ferroelectric ordering.[2–5] Such a magnetoelectric effect is very interesting from the point of view of fundamental physics, and could also lead to applications in spintronics and other fields.[6–13] A magnetoelectric device would allow one, for instance, to reverse magnetization by applying an electric field instead of a magnetic field.[14,15] However, there are very few single-phase magnetoelectric multiferroic materials due to chemical incompatibility between magnetism and ferroelectricity.[16] Besides that, in order to use the magnetoelectric effect in spintronic devices, it is needed to grow thin films of magnetoelectric materials.[9]

Among the magnetoelectric multiferroic materials suitable for applications, bismuth ferrite ($BiFeO_3$, BFO) has attracted much attention as it is perhaps the only known single-phase perovskite exhibiting coupled antiferromagnetic and ferroelectric ordering with transition temperatures higher than 300 K, which is essential for applications.[17–20] BFO's crystallization in the perovskite structure makes it compatible with many other functional compounds, and its large ferroelectric polarization (especially in thin films) makes it suitable for electronic devices.[21] Aiming at possible BFO-based devices, different techniques to synthesize high-quality BFO thin films have been exploited. Much efforts have been directed toward modifying and tuning the material's magnetic and electric properties through crystallinity, strain engineering,[22,23] ferroelectric and/or magnetic domain boundary control.[24,25] In this context, there is a need for methods compatible with the mass-production scenario and allowing fabrication of BFO-based systems with precise control over the film's properties, without the presence of spurious phases.

Several thin film deposition techniques have been used during the past decade such as pulsed laser deposition (PLD), chemical vapour deposition (CVD), atomic layer deposition (ALD), and radiofrequency (RF) magnetron sputtering. All of them, with their special features, have allowed epitaxial BFO thin films to be grown on single crystal substrates such as $SrTiO_3$ (STO), $NdScO_3$, $GdScO_3$, $DyScO_3$, etc. Nevertheless, the growing condition which allows a pure and stoichiometric BFO phase to be obtained is always very narrow, so that very small changes in the deposition parameters can lead to major changes in the film's properties and/or to the nucleation of spurious phases. In this sense, some groups have reported on unexpected magnetic moment in epitaxial thin films. For instance, Marchand *et al*. recently observed enhanced magnetization in ALD-grown BFO films which was attributed to the formation of magnetic domain walls and breaking of the helimagnetic antiferromagnetic order due to the phase confinement within the nanocrystalline morphology.[26] On the other hand, PLD-grown BFO films have been reported to present magnetic moment arising from parasitic phases formed mainly by iron oxides.[27,28]

In this work, we report on the structural and magnetic characterization of a series of epitaxial BFO thin films grown by low deposition rate RF magnetron sputtering. Initially, we present the structural and morphological characterization, performed by X-ray diffraction (XRD) and atomic force microscopy (AFM), which shows evidence of parasitic phase nucleation in some samples. In the sequence, we discuss the presence of anhysteretic or hysteretic magnetic behavior in magnetization measurements carried out by SQUID magnetometry. The origin of the magnetic moment, for each case, is attributed to different parasitic phases.

II. EXPERIMENTAL METHODS

The samples were grown in an AJA Orion sputtering system by sputtering a stoichiometric $BiFeO_3$ target. A pure

a)Electronic mail: thiago.mori@lnls.br

O_2 flux was kept in the chamber and a plasma was sustained by an impedance matched 100 W (RF) power. The base pressure prior to the deposition was lower than 8×10^{-8} Torr, whilst the deposition pressure was 30 mTorr. It is important to notice the unusual sputtering atmosphere (usually an atmosphere of $Ar + O_2$ is used for the reactive sputtering of oxides) and deposition pressure (usually a total pressure between 2 and 10 mTorr is used for magnetron sputtering deposition). These unusual conditions lead to a low deposition rate of the order of 1 Å/min, allowing the films to be epitaxially grown on single crystal STO (001) substrates. Samples were deposited at four different temperatures: 400 °C, 500 °C, 600 °C and 700 °C. Their thicknesses (as determined by X-ray reflectivity) are approximately 45 nm. The samples were post-annealed at the same temperature of the deposition, at a pressure of 75 Torr of pure oxygen, before bringing them to room temperature.

The structural characterization was performed by X-ray diffraction techniques. Some measurements were carried out on a Panalytical X'Pert Pro diffractometer with Cu K_α radiation, and others at the XRD2 beamline of the Brazilian Synchrotron Light Laboratory (LNLS) with a monochromatic beam of energy 7.5 keV. Standard Brag-Brentano ($\theta - 2\theta$) diffractograms were acquired to verify the out-of-plane crystallinity of the films and investigate parasitic phases. Rocking curves at the BFO (001) peak were collected to estimate the crystallite size through the Debye-Scherrer equation. X-ray reflectivity measurements, acquired in small incidence angles, provided information about the thicknesses of the samples. Reciprocal space maps (RSM) around the asymmetric (103) reflections of BFO and STO were measured to study the symmetry and in-plane strain. Atomic force microscopy images, taken on a Park NX10 microscope in the tapping mode, were acquired to study the local topography. The magnetic characterization was carried out on a Quantum Design MPMS® 3 VSM-SQUID magnetometer. The magnetization curves presented here have the diamagnetic signal of the substrate subtracted.

III. RESULTS AND DISCUSSION

X-ray diffractograms taken at the XRD2 beamline of the LNLS, with 7.5 keV photons in the Bragg-Brentano geometry ($\theta - 2\theta$), are shown in Fig. 1. The narrow STO (001) and (002) peaks are identified around $2\theta \approx 25°$ and $2\theta \approx 50°$, with the (001) and (002) BFO—in pseudocubic notation—just next to them (lower angle direction). The average crystallite sizes in the [001] direction were estimated from the FWHM of rocking curves collected at the BFO (001) peak position, by using the Debye-Scherrer equation. The values are about half of the nominal thicknesses, for all the samples, indicating that the epitaxial layer does not fill the entire structure. It could be forming a grainy film, or there could be nucleation of other phases instead. In fact, the diffractograms of the samples grown at higher temperatures present evidence of parasitic phases. The sample grown at 600 °C presents peaks around 34°, which can be indexed as related to the (220) and (002) planes of β–Bi_2O_3 (BO), and another one around 54° related to γ–Fe_2O_3 (FO). The peak around

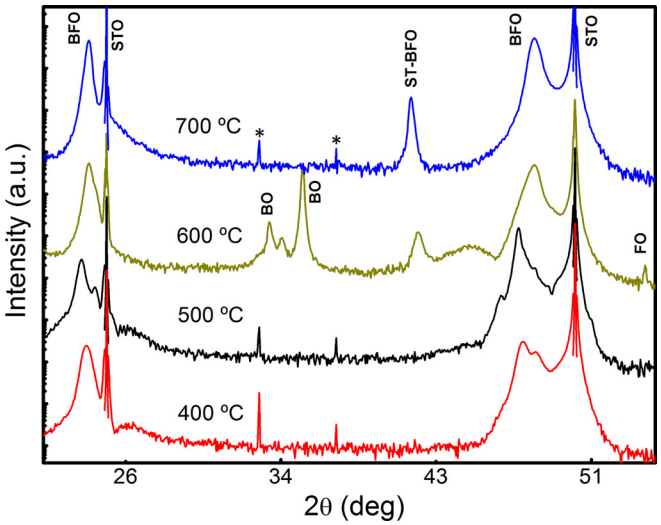

FIG. 1. X-ray diffractograms ($\theta - 2\theta$) for all samples, taken with 7.5 keV monochromatic radiation. The two narrow and very low intensity peaks around 33° and 37° (labelled as * in the figure) are assigned to multiple diffraction peaks of the substrate.

42°, which is present for the samples grown at higher temperatures (600 °C and 700 °C) is due to the formation of a tetragonal phase of BFO with a giant c/a ratio. Such a supertetragonal phase (ST-BFO), which would lead to a higher ferroelectric polarization,[29] is reported to be more stable than the monoclinic phase when BO is present.[30] The presence of these BO, FO and ST-BFO parasitic phases is accompanied by topographic features and unusual magnetic behavior that will be discussed further.

Looking at the diffractograms in Fig. 1, one can observe an evolution of the BFO (002) peak. Firstly, it is important to point out that the split of the peak suggests the presence of grains with different crystallographic properties. Starting from the lowest growing temperature, 400 °C, the peak evolutes from a distorted and split peak to a single and well-defined peak—accompanied by the ST-BFO peak around 42°—for the samples grown at higher temperatures. The unit cell of the samples grown at lower temperatures is significantly distorted, the c parameters (estimated from the most intense peak) being as high as 4.112 Å and 4.144 Å for samples grown at 400 °C and 500 °C, respectively, whilst the values for samples grown at 600 °C and 700 °C are 4.070 Å and 4.072 Å, respectively.

Figure 2 presents the reciprocal space maps (RSM) near the (103) reflections of the BFO film and the STO substrate. It is worth noting the improvement of the epitaxy of the c-oriented BFO films as the BFO (103) peak (in lower Q_z) becomes narrower and more intense for films grown at higher temperatures, corroborating the analysis of the $\theta - 2\theta$ measurements. Using the vertical line close to $Q_x = 1.61$ Å^{-1}—drawn in all RSM of Fig. 2 as a guide for the eyes, it can be observed that only the sample grown at 700 °C presents a strong compressive strain, with the in-plane cell parameter being 3.893 Å against 3.905 Å of the other samples which all follow the substrate parameter. The strain of this sample is estimated to be around 1.69%, whilst the strain of the others is around 1.38% (considering the BFO bulk in-plane cell

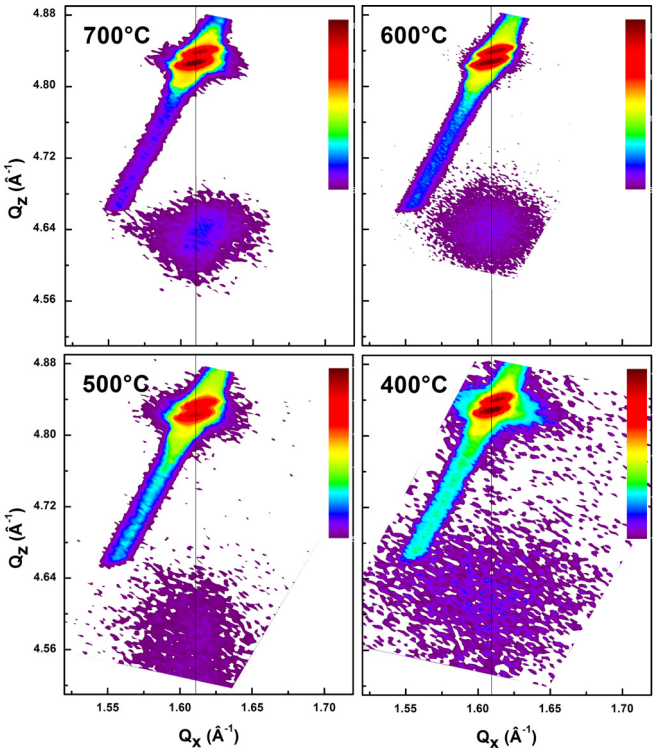

FIG. 2. Reciprocal space maps around the STO/BFO (103) reflections for BFO thin films deposited at 700 °C, 600 °C, 500 °C and 400 °C (from top left to bottom right). The RSM were acquired with Cuk_{α_1,α_2} radiation. The vertical line close to $Q_x = 1.61$ Å^{-1} is a guide for the eyes at the Q_z position of the STO substrate peak.

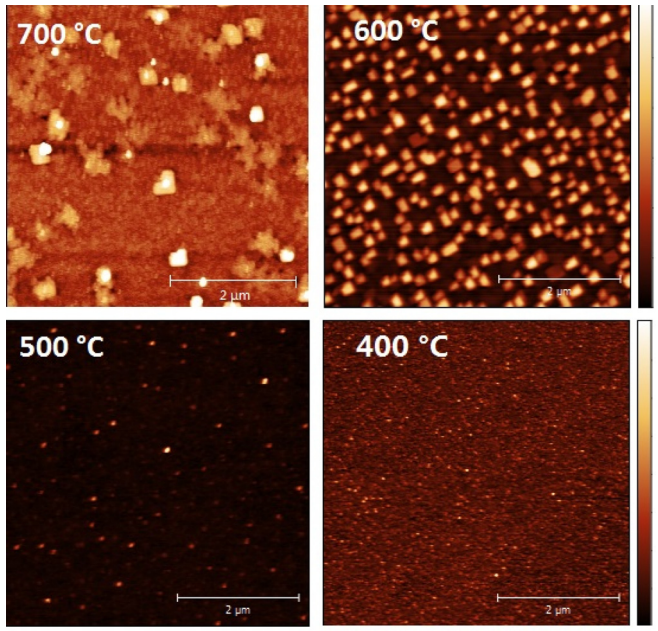

FIG. 3. Atomic force microscopy topographic images of samples grown at 700 °C, 600 °C, 500 °C and 400 °C (from top left to bottom right).

parameter as 3.96 Å). The strong compressive strain of the sample grown at 700 °C is related to the formation of the super-tetragonal phase, whose peak is stronger and located at a lower angle (stronger tetragonality) for the sample grown at 700 °C than that at 600 °C, and not present for the others.

It is possible to draw the following scenario from the XRD analysis: starting from the sample with the lowest epitaxy quality grown at 400 °C, the BFO quality is improved at 500 °C, but the beginning of the nucleation of a phase with higher tetragonality also takes place, which can be inferred analyzing the splitting and the shoulders on the left side of the (002) peak of this sample. The structural evolution to mixed BFO and ST-BFO phases keeps going on for sample 600 °C, and the epitaxy quality of BFO is much better (with a c/a ratio of 1.041), whilst the ST-BFO peak is clearly identified. Nevertheless, the nucleation of BO (and accompanying FO phases) is strongly favored at this temperature, which may also help with the stabilization of the ST-BFO phase. Furthermore, the sample 600 °C presents a broad peak around the region between ST-BFO and BFO peaks, suggesting that the transition from one phase to the other is not completed for this growing condition. Finally, the sample deposited at the highest temperature, 700 °C, presents an excellent quality BFO phase, with a c/a ratio of 1.047 due to the strong in-plane compressive strain caused by the coexistence of the supertetragonal phase, which is also epitaxial and well nucleated at this growing temperature.

The topography of the thin films is presented in Fig. 3. The samples grown at lower temperatures present smaller grains and low roughness, with the roughness average evaluated over an area of 2 × 2 μm^2 being less than 0.4 nm for samples grown at 400 °C and 500 °C. On the other hand, the samples grown at higher temperatures present some square-shaped features with heights of tens of nm. These features have already been reported and attributed to the nucleation of β–Bi_2O_3 outgrowths.[27,28,30,31] Indeed, by second harmonic Kelvin probe force microscopy (not shown), it was observed that there is a difference in the conductance between the square-shaped features and the rest of the surface, confirming that the regions are constituted by different phases (BO is much more conducting than BFO). The BO outgrowths are numerous and clearly observed on the surface of the sample grown at 600 °C, as expected due to the remarkable BO peaks that are present in the diffractogram of this sample. Although not presenting BO peaks in the diffractogram, samples grown at 500 °C and 700 °C also seem to present some degree of nucleation of bismuth oxide. This hypothesis is supported by the presence of some small square-shaped features in the topography of the sample grown at 500 °C (Fig. 3), and a few outgrowths observed in the AFM image of the sample grown at 700 °C (Fig. 3). We suggest that the BO phase nucleation is favored around 600 °C. In the case of the sample grown at 700 °C, it may appear during some stage of the growth mechanism to help the ST-BFO phase to nucleate, afterwards it is decomposed (possibly during the post-annealing) due to the volatility of Bi.

The remarkable presence of bismuth oxide on the surface of the sample grown at 600 °C suggests the formation of some iron oxide as well, so it does the peak around 54° in its diffractogram. Magnetization curves of all the samples, taken at room temperature, are shown in Fig. 4. All the samples, but the 600 °C one, present no measurable hysteretic behavior within the limits of the instrument. The small hysteretic behavior observed for other samples is due to the remanence of the magnet and has also been observed in

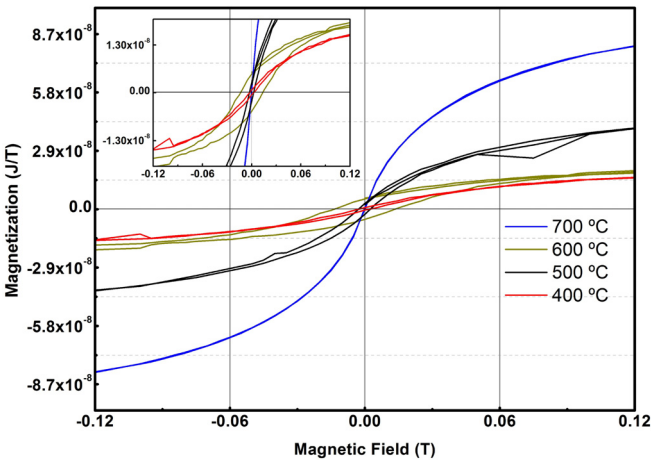

FIG. 4. Magnetic hysteresis loops measured at room temperature for samples grown at 400 °C, 500 °C, 600 °C and 700 °C.

paramagnetic reference samples. Besides that, zero field cooling (ZFC) and field cooling (FC) magnetization curves were also acquired (not shown here), and no vestige of superparamagnetic behavior was found for any sample. By its turn, the film deposited at 600 °C shows a significant coercive field even at room temperature. Such hysteretic ferromagnetic behavior, in accordance with the X-ray diffraction data, suggests the presence of some ferromagnetic iron oxide (likely γ–Fe_2O_3, a ferromagnetic phase with Curie temperature higher than 850 K). Considering the magnetic moment per formula unit of γ–Fe_2O_3 as 2.5 μ_B and its density as 4.9 g/cm^3, the volume of the FO parasitic phase necessary to generate the magnetic moment of the sample grown at 600 °C would be around 7% of the thin film volume. However, this volume of FO is surely overestimated, as we consider that all the magnetic moment is generated by this parasitic phase. This is not the case as other origins of magnetic moment may be present, and are not possible to be distinguished. Indeed, there is evidence of anhysteretic contribution to the magnetic moment, clearly observed in the sample grown at 700 °C, which will be discussed further.

The magnetic moment observed for the sample grown at 600 °C, together with the absence of either FO diffraction peaks or a magnetic coercive field in the structural and magnetometry analysis of the sample grown at 700 °C—which also presents a few BO outgrowths on the surface—strengthens the point that the coercivity of the sample grown at 600 °C is due to the presence of the iron oxide phase even though the total saturation magnetization may also be due to other contributions. This observation agrees with some results reported in the literature for BFO films grown by PLD.[27] Nevertheless, our low deposition rate films deposited by magnetron sputtering nucleate parasitic phases even for lower thicknesses than the expected according to this reference. This reference also suggests a role of the strain in stabilizing a metastable BFO phase detrimental to the stable BO one; however, the sputtered films reported here present the BO and FO parasitic phases together with strained metastable BFO. Moreover, the nucleation of iron oxide seems to not have any clear dependence on the presence of bismuth oxide.

Another kind of magnetism, being anhysteretic and presenting higher magnetic moment, is attributed to structural changes. This behavior is clearly observed for the sample grown at 700 °C (see Fig. 4), yet is probably present in the other samples as well. Indeed, there are several reports about the changes in the magnetic properties of BFO accompanying structural modifications.[32,33] Such structural changes can arise, for instance, from doping, size confinements in nanostructures or due to the development of mixed BFO phases that can lead to the distortion of the spin cycloid structure.[32,34–40] The latter one is clearly the case of the sample grown at 700 °C, according to its diffraction pattern, which evidences the coexistence of two well-defined distinct phases of BFO.

Starting from the lowest temperature, the sample grown at 400 °C—with lower epitaxy quality—presents a very low magnetic moment. Increasing the growing temperature, the sample grown at 500 °C shows a little higher moment, with the BFO phase quality getting improved, and some features in the XRD suggesting the very beginning of the ST-BFO phase nucleation. The structural disorder caused by the nucleating stage of the ST-BFO phase and the remarkable presence of non-magnetic BO make the magnetic moment of the sample grown at 600 °C smaller even though the presence of FO (in a very small quantity) leads to hysteretic ferromagnetic behavior. In turn, when the growing temperature is as high as 700 °C, the stabilization via strain of the ST-BFO phase is responsible for the higher magnetic moment observed in this sample. This result is consistent with data reported by other authors. For instance, in Ref. 34, the authors report on the enhancement of the rhombohedral BFO magnetization as a consequence of a piezomagnetic coupling to the adjacent tetragonal-like phase and epitaxial constraint.

It is worth mentioning that the presence of Fe^{2+} in oxygen deficient BFO films has also been reported to lead to a high magnetic moment in epitaxial thin films free of spurious phases.[21,41] However, the high oxygen partial pressure in the chamber during the deposition of the samples reported here, as well as the post-annealing carried out at even higher pressures, is expected to preclude the reduction of the film. Nevertheless, the presence of oxygen vacancies is hard to be measured experimentally, and magnetic moment coming from the presence of Fe^{2+} in the BFO structure cannot be totally disregarded even though it is very unlikely.

IV. CONCLUSION

In summary, we have managed to grow epitaxial BFO thin films by RF magnetron sputtering in an unusual environment of high partial pressure and pure O_2. The samples presented an evolution of the quality of epitaxy with the deposition temperature. The spurious β–Bi_2O_3 phase is present in samples deposited at higher temperatures and is shown by square-shaped outgrowths on the surface. This parasitic phase is known to have higher conductance, and could be a problem to the application of BFO thin films in ferroelectric and magnetoelectric devices. The coexistence of the super-tetragonal phase of BFO is also observed in the same samples. The XRD analysis of the sample grown at 600 °C also presents evidence of γ–Fe_2O_3 nucleation. As it is the only sample to present clear hysteretic

ferromagnetic behavior, the origin of the coercive field in this film is attributed to the small nucleation of the iron oxide spurious phase. Nevertheless, the sample grown at 700 °C presents a strong anhysteretic magnetic behavior, with high saturation magnetization and no indication of spurious iron oxide phases; therefore, the origin of its magnetic moment is attributed to the coexistence of two mixed BFO phases. In mixed phase nanostructures, the BFO film nanocrystalline morphology is prominently relevant to their magnetic properties.

ACKNOWLEDGMENTS

This work was supported by FAPESP (Project No. 2012/51198-2). Some of the XRD measurements were performed at the XRD2 beamline of the LNLS/CNPEM under Project Nos. 20150162 and 20160908. The authors thank the LNNano/CNPEM for XRD/XRR, AFM and sputtering facilities, the LIEC/UFSCar for the SQUID measurements, and M. M. Soares for important discussions regarding the structural characterization. P.S. thanks FAPESP for financial support (Project No. 2012/18397-1). J.C.C. acknowledges support from CNPq (Project No. 309354/2015-3).

[1]H. Schmid, Ferroelectrics **162**, 317 (1994).
[2]M. Fiebig, J. Phys. D: Appl. Phys. **38**, R123 (2005).
[3]N. A. Spaldin and M. Fiebig, Science **309**, 391 (2005).
[4]D. I. Khomskii, J. Magn. Magn. Mater. **306**, 1 (2006).
[5]W. Eerenstein, N. D. Mathur, and J. F. Scott, Nature **442**, 759 (2006).
[6]S. Fusil, V. Garcia, A. Barthélémy, and M. Bibes, Annu. Rev. Mater. Res. **44**, 91 (2014).
[7]S.-W. Cheong and M. Mostovoy, Nat. Mater. **6**, 13 (2007).
[8]S. Dong, J.-M. Liu, S.-W. Cheong, and Z. Ren, Adv. Phys. **64**, 519 (2015).
[9]R. Ramesh and N. A. Spaldin, Nat. Mater. **6**, 21 (2007).
[10]C. W. Nan, M. I. Bichurin, S. Dong, D. Viehland, and G. Srinivasan, J. Appl. Phys. **103**, 031101 (2008).
[11]A. Rodzinski, R. Guduru, P. Liang, A. Hadjikhani, T. Stewart, E. Stimphil, C. Runowicz, R. Cote, N. Altman, R. Datar, and S. Khizroev, Sci. Rep. **6**, 20867 (2016).
[12]R. K. Kotnala, R. Gupta, and S. Chaudhary, Appl. Phys. Lett. **107**, 082908 (2015).
[13]R. Gupta, S. Chaudhary, and R. K. Kotnala, ACS Appl. Mater. Interfaces **7**, 8472 (2015).
[14]J. T. Heron, J. L. Bosse, Q. He, Y. Gao, M. Trassin, L. Ye, J. D. Clarkson, C. Wang, J. Liu, S. Salahuddin, D. C. Ralph, D. G. Schlom, J. Iñiguez, B. D. Huey, and R. Ramesh, Nature **516**, 370 (2014).
[15]T. Zhao, A. Scholl, F. Zavaliche, K. Lee, M. Barry, A. Doran, M. P. Cruz, Y. H. Chu, C. Ederer, N. A. Spaldin, R. R. Das, D. M. Kim, S. H. Baek, C. B. Eom, and R. Ramesh, Nat. Mater. **5**, 823 (2006).
[16]N. A. Hill, J. Phys. Chem. B **104**, 6694 (2000).
[17]M. Guennou, M. Viret, and J. Kreisel, C.R. Phys. **16**, 182 (2015).
[18]J. F. Scott, NPG Asia Mater. **5**, 72 (2013).
[19]G. Catalan and J. F. Scott, Adv. Mater. **21**, 2463 (2009).
[20]D. Sando, B. Xu, L. Bellaiche, and V. Nagarajan, Appl. Phys. Rev. **3**, 011106 (2016).
[21]J. Wang, J. B. Neaton, H. Zheng, V. Nagarajan, S. B. Ogale, B. Liu, D. Viehland, V. Vaithyanathan, D. G. Schlom, U. V. Waghmare, N. A. Spaldin, K. M. Rabe, M. Wuttig, and R. Ramesh, Science **299**, 1719 (2003).
[22]A. Agbelele, D. Sando, C. Toulouse, C. Paillard, R. D. Johnson, R. Rüffer, A. F. Popkov, C. Carrétéro, P. Rovillain, J.-M. Le Breton, B. Dkhil, M. Cazayous, Y. Gallais, M.-A. Méasson, A. Sacuto, P. Manuel, A. K. Zvezdin, A. Barthélémy, J. Juraszek, and M. Bibes, Adv. Mater. **29**, 1602327 (2017).
[23]C.-Y. Kuo, Z. Hu, J. C. Yang, S.-C. Liao, Y. L. Huang, R. K. Vasudevan, M. B. Okatan, S. Jesse, S. V. Kalinin, L. Li, H. J. Liu, C.-H. Lai, T. W. Pi, S. Agrestini, K. Chen, P. Ohresser, A. Tanaka, L. H. Tjeng, and Y. H. Chu, Nat. Commun. **7**, 12712 (2016).
[24]T. E. Quickel, L. T. Schelhas, R. A. Farrell, N. Petkov, V. H. Le, and S. H. Tolbert, Nat. Commun. **6**, 6562 (2015).
[25]G. Catalan, J. Seidel, R. Ramesh, and J. F. Scott, Rev. Mod. Phys. **84**, 119 (2012).
[26]B. Marchand, P. Jalkanen, V. Tuboltsev, M. Vehkamäki, M. Puttaswamy, M. Kemell, K. Mizohata, T. Hatanpää, A. Savin, J. Räisänen, M. Ritala, and M. Leskelä, J. Phys. Chem. C **120**, 7313 (2016).
[27]H. Béa, M. Bibes, S. Fusil, K. Bouzehouane, E. Jacquet, K. Rode, P. Bencok, and A. Barthélémy, Phys. Rev. B -Condens. Matter Mater. Phys. **74**, 020101 (2006).
[28]H. Béa, M. Bibes, A. Barthélémy, K. Bouzehouane, E. Jacquet, A. Khodan, J. P. Contour, S. Fusil, F. Wyczisk, A. Forget, D. Lebeugle, D. Colson, and M. Viret, Appl. Phys. Lett. **87**, 072508 (2005).
[29]A. J. Hatt, N. A. Spaldin, and C. Ederer, Phys. Rev. B -Condens. Matter Mater. Phys. **81**, 054109 (2010).
[30]H. Liu, P. Yang, K. Yao, K. P. Ong, P. Wu, and J. Wang, Adv. Funct. Mater. **22**, 937 (2012).
[31]H. Toupet, F. Le Marrec, J. Holc, M. Kosec, P. Vilarhino, and M. G. Karkut, J. Magn. Magn. Mater. **321**, 1702 (2009).
[32]J. Wu, Z. Fan, D. Xiao, J. Zhu, and J. Wang, Prog. Mater. Sci. **84**, 335 (2016).
[33]D. Kim and D. Lim, J. Korean Phys. Soc. **62**, 734 (2013).
[34]Q. He, Y.-H. Chu, J. T. Heron, S. Y. Yang, W. I. Liang, C. Y. Kuo, H. J. Lin, P. Yu, C. W. Liang, R. J. Zeches, W. C. Kuo, J. Y. Juang, C. T. Chen, E. Arenholz, A. Scholl, and R. Ramesh, Nat. Commun. **2**, 225 (2011).
[35]Y. Wang, J. Li, J. Chen, and Y. Deng, J. Appl. Phys. **113**, 103904 (2013).
[36]N. T. Huong, S.-H. Lee, T. Atabaev, M. Kurisu, and N. H. Hong, Adv. Condensed Matter Phys. **2015**, 371802 (2015).
[37]Y. Wei, X. Wang, J. Jia, and X. Wang, Ceram. Int. **38**, 3499 (2012).
[38]K. Singh, A. Gautam, K. Sen, R. K. Kotnala, M. Kumar, P. Gautam, and M. Singh, J. Appl. Phys. **109**, 123911 (2011).
[39]F. Yan, T. J. Zhu, M. O. Lai, and L. Lu, Scr. Mater. **63**, 780 (2010).
[40]S. Pradhan and B. Roul, Phys. B: Condens. Matter **407**, 2527 (2012).
[41]W. Eerenstein, F. D. Morrison, J. Dho, M. G. Blamire, J. F. Scott, and N. D. Mathur, Science **307**, 1203 (2005).